A M2L2 Redox-Active Metalla-Macrocycle Based on Electron-Rich 9-(1,3-Dithiol-2-ylidene)Fluorene

Serhii Krykun, Magali Allain, Vincent Carré, Frédéric Aubriet, Zoia Voitenko, Sébastien Goeb, Marc Sallé

inorganics

MDPI

Communication

A M_2L_2 Redox-Active Metalla-Macrocycle Based on Electron-Rich 9-(1,3-Dithiol-2-ylidene)Fluorene

Serhii Krykun [1,2], Magali Allain [1], Vincent Carré [3], Frédéric Aubriet [3], Zoia Voitenko [2], Sébastien Goeb [1,*] and Marc Sallé [1,*]

1 Laboratoire MOLTECH-Anjou, Université d'Angers, CNRS UMR 6200, 2 bd Lavoisier, 49045 Angers CEDEX, France; serhii.krykun@etud.univ-angers.fr (S.K.); magali.allain@univ-angers.fr (M.A.)
2 Taras Shevchenko National University of Kyiv, 64/13 Volodymyrska st., 01033 Kyiv, Ukraine; z_voitenko@ukr.net
3 LCP-A2MC, FR 2843 Institut Jean Barriol de Chimie et Physique Moléculaires et Biomoléculaires, FR 3624 Réseau National de Spectrométrie de Masse FT-ICR à très haut champ, Université de Lorraine, ICPM, 1 boulevard Arago, 57078 Metz CEDEX 03, France; vincent.carre@univ-lorraine.fr (V.C.); frederic.aubriet@univ-lorraine.fr (F.A.)
* Correspondence: sebastien.goeb@univ-angers.fr (S.G.); marc.salle@univ-angers.fr (M.S.)

Received: 10 April 2018; Accepted: 26 April 2018; Published: 3 May 2018

Abstract: A redox-active M_2L_2 metalla-macrocycle is depicted, of which construction has been achieved through coordination driven self-assembly from an electron-rich 9-(1,3-dithiol-2-ylidene)fluorene bis-pyridyl ligand and a *cis*-blocked square planar palladium complex (Pd(dppf)OTf_2, dppf = 1,1′-Bis(diphenylphosphino)ferrocene). The resulting metalla-macrocycle has been fully characterized in solution, as well as in the solid state (X-ray crystal structure). Its electronic properties show that both constitutive ligands can be oxidized independently through a one-electron process.

Keywords: supramolecular chemistry; self-assembly; coordination compound; metalla-macrocycle; 9-(1,3-dithiol-2-ylidene)Fluorene; redox-active compound

1. Introduction

Since the pioneering example reported by Fujita [1], a plethora of ever more sophisticated metalla-rings and -cages constructed by coordination-driven self-assembly have been reported [2–7]. This methodology takes advantage of the labile character of the coordination bonds to produce high yields and single step thermodynamically stable architectures, with complex structures that would be challenging to reach through traditional organic chemistry. These self-assembled architectures are usually characterized by an internal cavity that can be exploited in guest encapsulation leading to various applications such as chemistry in confined space [8,9] or drug delivery [10–12]. Beyond the synthetic challenge in preparing such objects, there is a strong interest in providing them with functionality, as encountered with recently described stimuli responsive rings and cages structures [13–16]. In this context, the preparation of redox-active metalla-rings/cages which allow a redox control over their overall charge appears relevant [17,18] and we described recently the first examples of electron-rich redox-active coordination cages capable of modulating their encapsulation properties through a redox stimulus [19,20].

In the course of our research related to the preparation of electron-rich self-assemblies [17,19–26], we have recently demonstrated that the 9-(1,3-dithiol-2-ylidene)fluorene moiety, which is known to be readily and reversibly oxidized into a cation-radical [27,28], can be used as a building-block for the construction of electro-active self-assembled cages [29]. In line with this work, we describe herein the synthesis of an original electron-rich M_2L_2 metalla-macrocycle constructed from the *cis*-blocked Pd(dppf)OTf_2

(dppf = 1,1′-Bis(diphenylphosphino)ferrocene) acceptor and a 9-(1,3-dithiol-2-ylidene)fluorene ligand (**L4Pyr**) that incorporates two pyridin-4-yl units in the corresponding 3,6-positions.

2. Results and Discussion

The synthesis of ligand **L4Pyr** (Scheme 1) was carried out in two steps from 3,6-dibromo-9H-fluoren-9-one **1** adapted from our previous described procedure [29]. A pallado-catalyzed Sonogashira cross coupling reaction with 4-ethynylpyridine affords the new compound **2** with 59% yield upon microwave irradiation. The subsequent Horner–Wardsworth–Emmons reaction was carried out with the 4,5-bis(hexylsulfanyl)-1,3-dithiol phosphonate ester **3** to afford the target new ligand **L4pyr** with 75% yield after purification.

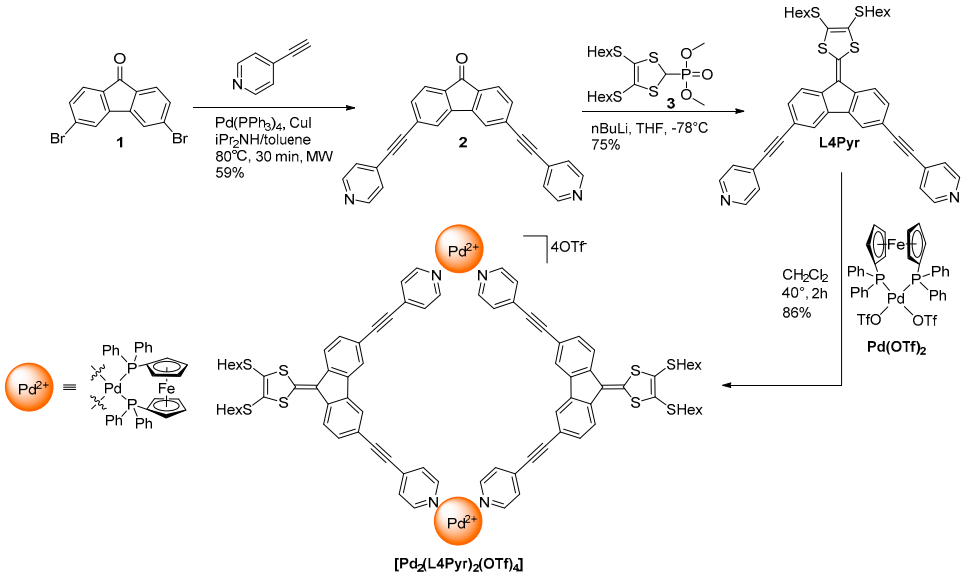

Scheme 1. Synthesis of ligand **L_4Pyr** and metalla-macrocycle [**Pd_2(L4Pyr)$_2$(OTf)$_4$**].

Slow evaporation of a CH_2Cl_2/EtOH solution of ligand **L4Pyr** allowed for obtaining single crystals suitable for X-Ray analysis. The corresponding solid-state crystal structure is depicted in Figure 1. Remarkably, the presence of two hexylsulfanyl chains did not prevent crystallization. As for its pyridin-3-yl homologous ligand [29], **L4Pyr** shows a nearly planar geometry with a slight folding of the dithiole rings (6° across the S···S vector) and a slight twist of the pyridine units relatively to the central planar fluorene core with angles of ca. 4.1°. As expected, the angle observed between both ethynyl axes is close to 90°, an angle that is therefore extended to the coordination angle provided by both nitrogen atoms of the pyridine fragments.

Reaction between ligand **L4Pyr** and complex Pd(dppf)OTf$_2$ (Scheme 1) was carried out in CD_2Cl_2 and followed by ^{1}H-NMR. After 2 h, the reaction converged to a unique structure that could be isolated by precipitation with Et_2O. The resulting ^{1}H-NMR spectrum exhibits a single set of well resolved signals as anticipated from a symmetrical discrete self-assembly (Figure 2). H_4 and H_5 signals are upfield shifted compared to ligand **L4Pyr** due to through-space interactions between the coligand phenyl units (dppf) and the pyridyl groups, confirming coordination to the metal center [22,24]. A ^{1}H-NMR DOSY experiment revealed a single set of signals that confirms the formation of a unique discrete species. From the corresponding diffusion value of $D = 10^{-10}$ m^2·s^{-1}, a hydrodynamic radius of ca. 10 Å was estimated from the Stokes-Einstein equation (T = 298 K) [30], a value which is compatible with the formation of the expected tetracationic M_2L_2 architecture [**Pd_2(L4Pyr)$_2$(OTf)$_4$**] [31,32].

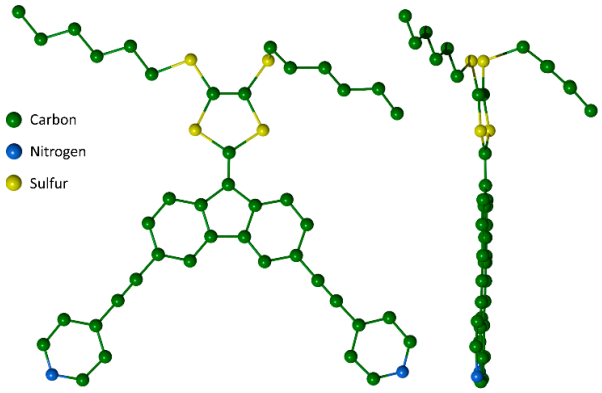

Figure 1. X-ray crystal structure of ligand **L4Pyr**.

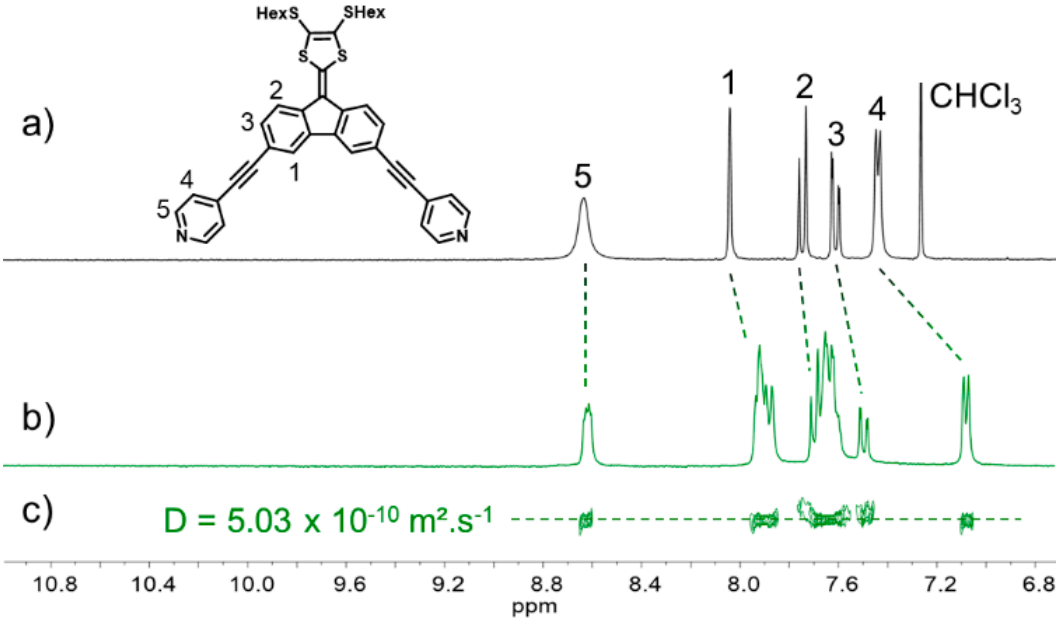

Figure 2. ^{1}H-NMR spectra (aromatic region) of (**a**) ligand **L4Pyr** ($CDCl_3$), (**b**) metalla-macrocycle **[Pd$_2$(L4Pyr)$_2$(OTf)$_4$]** (CD_2Cl_2) and (**c**) corresponding ^{1}H-NMR DOSY spectra (related to (**b**)).

High resolution ESI-FTICR-MS spectrometry experiments were carried out to confirm the stoichiometry of the discrete self-assembled complex. Surprisingly, regardless of the instrumental conditions, the solvent and the concentration (10^{-5} M < C < 10^{-3} M), signal corresponding to the expected M_2L_2 ([**Pd$_2$(L4Pyr)$_2$(OTf)$_4$**] − 2OTf]$^{2+}$; m/z = 1510.1598) was accompanied by mass peaks due to higher nuclearity assemblies. In particular are observed M_4L_4 ([[**Pd$_4$(L4Pyr)$_4$(OTf)$_8$**] − 3OTf]$^{3+}$; m/z = 2064.1986) and sometimes M_6L_6 species (see Figure 3 and Figure S8 for an illustrative example), whose relative abundances diminish with aggregates size. In accordance with the previously-mentioned DOSY experiment, such MS spectra suggest the presence in solution of M_2L_2 species that aggregate upon ESI to form dimers and trimers, a phenomenon that is known to occur at high concentration and with soft ionization conditions [33].

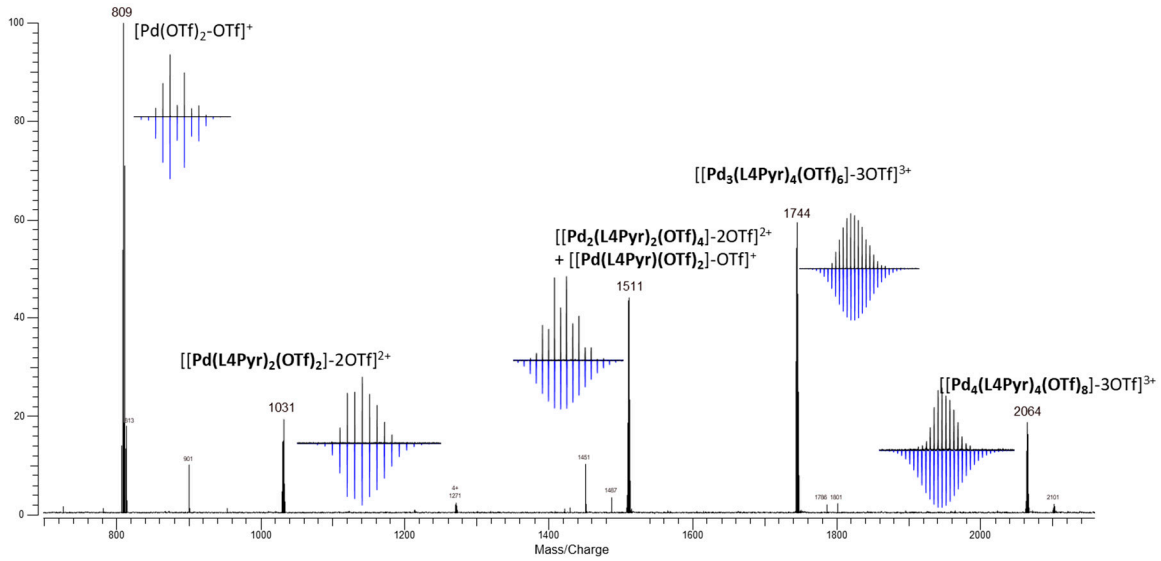

Figure 3. ESI-FTICR mass spectrum of metalla-macrocycle **[Pd$_2$(L4Pyr)$_2$(OTf)$_4$]** in CH_2Cl_2/CH_3NO_2 (9/1) (C = 10^{-3} M), in black experimental isotopic pattern, in blue theoretical isotopic pattern.

Fortunately, single crystals could be grown by slow diffusion of MeOtBu in a CH_2Cl_2 solution containing **[Pd$_2$(L4Pyr)$_2$(OTf)$_4$]** (C = 1 mM). X-ray crystallography analyses confirmed unambiguously the expected M_2L_2 stoichiometry (Figure 4). Two independent discrete assemblies were found in the crystal packing (Figure 4a). They exhibit a similar configuration but differ essentially by the dihedral angle between both dithiafulvenyl mean planes (DTF) (88.7° and 58.1 for blue and turquoise species respectively). The two forms interact through π–π interactions between their respective DTF units with interplanar distance of 3.45 Å, as well as CH–π interactions between DTF units and SHex chains. The geometrical characteristics of the constitutive **L4Pyr** ligand are mostly preserved in the metalla-macrocycle despite the fact that the average twisting between pyridine units and fluorene core increases to 12.5°.

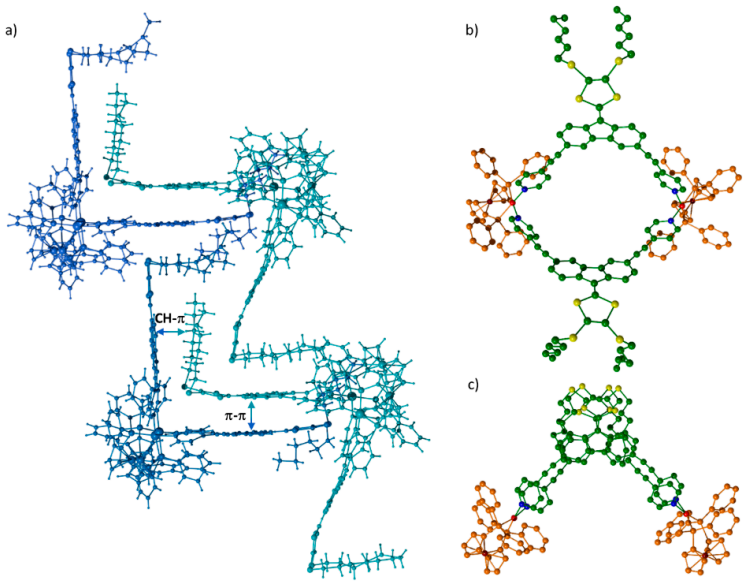

Figure 4. X-ray crystal structure of **[Pd$_2$(L4Pyr)$_2$(OTf)$_4$]**, (**a**) crystal packing showing two independent discrete assemblies (blue and turquoise respectively), (**b**) top view and (**c**) lateral view of turquoise metalla-macrocycle (related to (**a**)). Counter anions, solvent molecules and hydrogen atoms (**b**,**c**) omitted for clarity.

UV-vis absorption spectra of ligand **L4Pyr** and metalla-macrocycle **[Pd$_2$(L4Pyr)$_2$(OTf)$_4$]** were recorded in dichloromethane at C = 1.5 × 10^{-5} M (Figure 5). The absorption profile of **L4Pyr** reveals two high energy absorption bands at 290 nm and 350 nm attributed to π–π* transitions located on the fluorene and pyridines units respectively, whereas the intense low energy band at 460 nm (ε = 46,000 M^{-1}·cm^{-1}) shows an ICT character from the HOMO localized on the DTF unit to the LUMO of the electron accepting pyridyles [34]. The absorption spectrum of **[Pd$_2$(L4Pyr)$_2$(OTf)$_4$]** complex exhibits a similar profile with maxima shifted to lower energy (λ_{max} = 483 nm) as expected from metal coordination, and ε values twice higher (ε = 102,000 M^{-1}·cm^{-1}) accordingly to the metalla-ring formula.

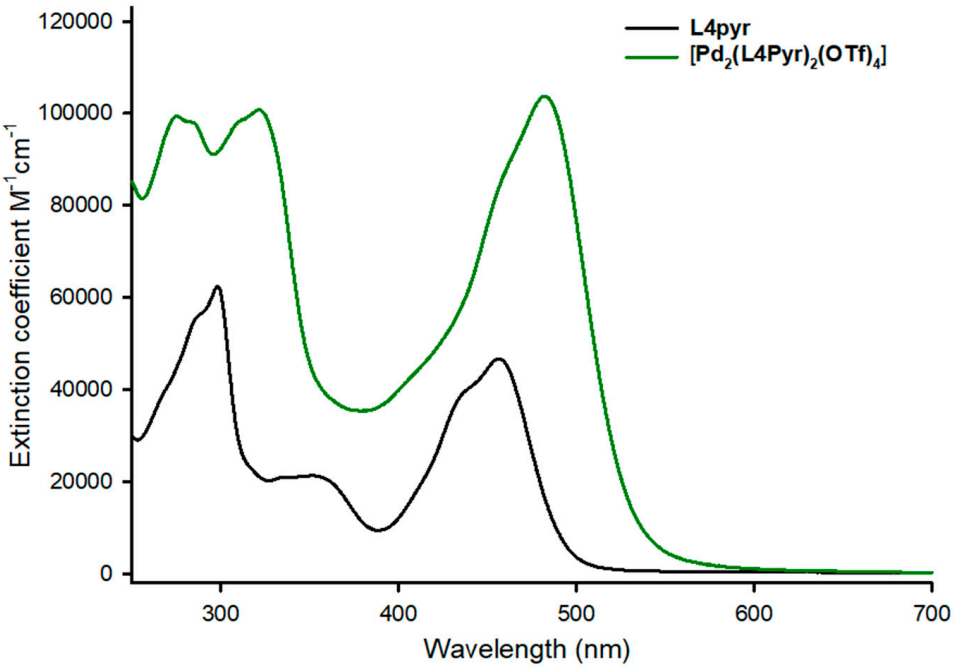

Figure 5. UV-vis absorption spectra of ligand **L4Pyr** and metalla-macrocycle **[Pd$_2$(L4Pyr)$_2$(OTf)$_4$]**, r.t. (C = 1.5 × 10^{-5} M in CH_2Cl_2).

The electrochemical properties of ligand **L4Pyr** and complex **[Pd$_2$(L4Pyr)$_2$(OTf)$_4$]** were studied by cyclic voltammetry in CH_3CN/CH_2Cl_2 (1/1, *v*/*v*) (Figure 6). Ligand **L4Pyr** exhibits one reversible oxidation wave at E_1^{ox} = 0.57 V vs. Fc/Fc^+ which is attributed to the formation of the DTF radical-cation [27,28]. This potential is higher by 0.15 V compared to the one of the homologous ligand bearing two pyridine-3-yl units [29]. This behavior is in accordance to previous observations on pyridine-4-yl (vs. pyridine-3-yl) mono substituted TTF based ligands [35] and accounts for the respective electronic effect of the nitrogen atom. The corresponding metalla-cycle complex presents two reversible oxidation waves. The first one, anodically shifted by 20 mV compared to the uncoordinated ligand is attributed to the oxidation of DTF units (E_1^{ox} = 0.59 V vs. Fc/Fc^+) while the second is centered on the ferrocene moieties at E_2^{ox} = 0.83 V, both processes presenting similar intensities. Altogether, this behavior suggests that both organic redox active DTF units behave independently upon oxidation to their radical cation state and that they do not interact electronically.

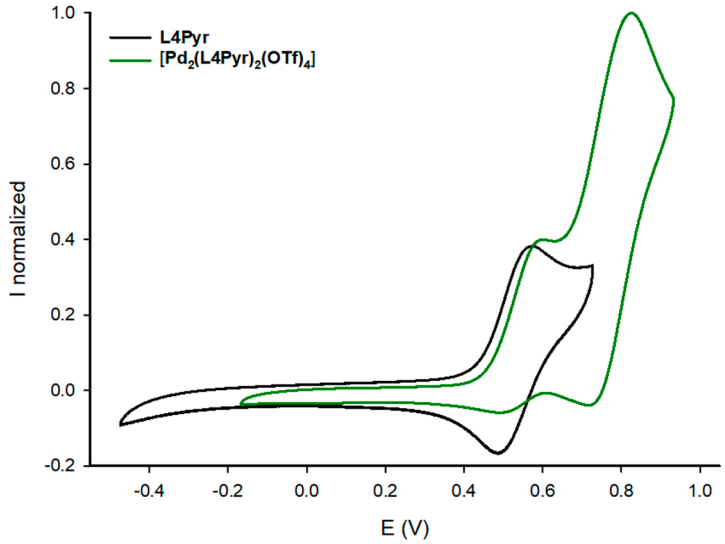

Figure 6. Normalized cyclic voltammograms of ligand **L4Pyr** and metalla-ring **[Pd$_2$(L4Pyr)$_2$(OTf)$_4$]** (C = 10^{-3} M, CH_3CN/CH_2Cl_2, 0.1 M nBu_4NPF_6, 100 mV·s^{-1}, Pt) V vs. Fc/Fc^+.

3. Materials and Methods

3.1. Chemicals

Compound **1** [36] and **3** [37] were synthetized as described in the literature. All reagents were of commercial reagent grade and were used without further purification. Silica gel chromatography was performed with a SIGMA Aldrich Chemistry SiO_2 (pore size 60 Å, 40–63 μm technical grades) (Sigma-Aldrich, Steinheim, Germany).

3.2. Instrumentation

The 300 (^{1}H), 75.5 (^{13}C) MHz NMR spectra were recorded at room temperature using perdeuterated solvents as internal standards (^{1}H on a NMR Bruker Avance III 300 spectrometer (Bruker, Wissembourg, France). MALDI-TOF-MS spectra were recorded on a MALDI-TOF Bruker Biflex III instrument (Bruker, Wissembourg, France) using a positive-ion mode. ESI-FTICR spectra were performed in positive detection mode on a IonSpec (Agilent, Santa-Clara, CA, USA), 9,4 T hybride ESI q-Q-q. Cyclic voltammetry experiments were carried out on a BioLogic SP-150 potentiostat (BioLogic, Seyssinet-Pariset, France).

3.3. Experimental Procedure and Characterization Data

3.3.1. Synthesis of 3,6-bis(Pyridin-4-ylethynyl)-9H-fluoren-9-one (**2**)

To an argon degassed solution of 3,6-dibromo-9H-fluoren-9-one **1** (100 mg, 0.30 mmol) and 3-ethynylpyridine (122 mg, 1.18 mmol, 4 equiv.) in a mixture of diisopropylamine/toluene 1/1 (4 mL) placed in a microwave tube, $Pd(PPh_3)_4$ (68 mg, 0.06 mmol, 0.2 equiv.) and CuI (11 mg, 0.06 mmol, 0.2 equiv.) were added. The sealed tube was irradiated for 30 min at a constant 250 W and the solvent was evaporated under vacuum. The residue was then treated with water and extracted with dichloromethane. The organic extracts were washed with water and dried over magnesium sulfate. The solvent was evaporated under vacuum. A chromatography column on silica gel was performed using a gradient of eluent: from dichloromethane/petroleum ether (80/20) to dichloromethane/methanol (98/2). The residue was further purified by recrystallization in dichloromethane/pentane. Compound **2** was obtained as yellow powder 67 mg, 59% yield. ^{1}H-NMR (300 MHz, $CDCl_3$) δ 8.66 (d, *J* = 5.8 Hz, 4H), 7.73–7.70 (m, 4H), 7.54 (dd, *J* = 7.6, 1.1 Hz, 2H), 7.42 (dd,

J = 4.6, 1.4 Hz, 4H); ^{13}C-NMR (75.5 MHz, $CDCl_3$) δ 191.64, 149.95, 143.65, 134.30, 133.28, 130.67, 128.62, 125.59, 124.57, 123.71, 92.93, 90.05; FAB-HRMS: found: 382.1099, calculated: 382.1106.

3.3.2. Synthesis of Ligand **L4Pyr**

n-Butyllithium (0.15 mL, 0.37 mmol, 1.6 M, 1.5 equiv.) was slowly added to a solution of phosphonate ester **3** (165 mg, 0.37 mmol, 1.5 equiv.) in anhydrous tetrahydrofuran (10 mL) at −78 °C. The mixture was stirred for one hour at −78 °C and a suspension of 3,6-bis(pyridin-3-ylethynyl)-9H-fluoren-9-one 2 (95 mg, 0.25 mmol, 1 equiv.) in anhydrous tetrahydrofuran (10 mL) at −78 °C was added via cannula. The mixture was stirred for 1 h at −78 °C and overnight at room temperature. The solvent was removed under vacuum. The residue was then treated with water and extracted with dichloromethane. The organic extracts were washed with water, and dried over magnesium sulfate. The solvent was removed under vacuum. A chromatography column on silica gel was performed using a gradient of eluent: petroleum ether/dichloromethane (50/50) to dichloromethane/methanol (98/2). The residue was further purified by recrystallization dichloromethane/methanol. Ligand **L4Pyr** was obtained as orange crystals (132 mg, 75%). ^{1}H-NMR (300 MHz, $CDCl_3$) δ 8.63 (s, 4H), 8.06–7.99 (m, 2H), 7.74 (d, *J* = 8.2 Hz, 2H), 7.61 (dd, *J* = 8.2, 1.5 Hz, 2H), 7.43 (d, *J* = 5.3 Hz, 4H), 2.98 (t, *J* = 7.3 Hz, 4H), 1.71 (m, 4H), 1.47 (m, 4H), 1.32 (m, 8H), 0.90 (t, *J* = 7.0 Hz, 6H) ; ^{13}C-NMR (75.5 MHz, $CDCl_3$) δ 149.58, 142.70, 137.52, 136.81, 131.86, 130.92, 129.64, 125.63, 123.39, 122.70, 119.49, 118.64, 95.12, 87.17, 36.78, 31.35, 30.96, 28.26, 22.56, 14.05; FAB-HRMS: found: 700.2082, calculated: 700.2074.

3.3.3. Synthesis of Metalla-Macrocycle [$\mathbf{Pd_2(L4Pyr)_2(OTf)_4}$]

A mixture of ligand **L4Pyr** (7.01 mg, 0.01 mol) and Pd(dppf)OTf_2 (9.57 mg, 0.01 mol) in CH_2Cl_2 (1 mL) were stirred at 40 °C for 2 h. The red solution was cooled down to room temperature, and Et_2O (5 mL) was then added. The mixture was centrifuged and the resulting solid was dried in vacuum to afford [$\mathbf{Pd_2(L4Pyr)_2(OTf)_4}$] as a red powder (14.3 mg, 86%). ^{1}H-NMR (300 MHz, CD_2Cl_2) δ 8.69–8.44 (m, 8H), 8.01–7.78 (m, 20H), 7.64 (m, 28H), 7.49 (dd, *J* = 8.2, 1.6 Hz, 4H), 7.07 (dt, *J* = 5.3, 1.3 Hz, 8H), 4.80 (s, 10H), 4.63 (s, 10H), 2.94 (t, *J* = 7.3 Hz, 8H), 1.64 (m, 8H), 1.41 (m, 8H), 1.27 (m, 16H), 0.85 (m, 12H); ^{13}C-NMR (75.5 MHz, $CDCl_3$) δ 150.06, 144.93, 137.79, 136.21, 134.89, 134.15, 134.05, 132.84, 130.76, 129.79, 129.70, 127.78, 127.50, 127.04, 123.96, 122.43, 122.33, 119.77, 118.64, 117.22, 99.73, 85.66, 76.83, 76.77, 76.73, 75.35, 75.29, 70.10, 70.06, 69.58, 69.54, 36.55, 31.14, 29.59, 28.02, 22.38, 13.63; FTICR-HRMS (*m*/*z*), [$[\mathbf{Pd_2L4pyr_2}]^{4+} - 2TfO^-]^{2+}$: found: 1510.1598, calculated 1510.1660.

3.4. X-ray Crystallographic Analysis

X-ray single-crystal diffraction data for **L4Pyr** and [$\mathbf{Pd_2(L4Pyr)_2(OTf)_4}$] were collected at 150 K on an Agilent Technologies SuperNova diffractometer equipped with an Atlas CCD detector and micro-focus Cu Kα radiation (λ = 1.54184 Å). Both structures were solved by direct methods and refined on F^2 by full matrix least-squares techniques using *SHELX* (G.M. Sheldrick, 2013–2016) package. All non-hydrogen atoms were refined anisotropically and the H atoms were included in the calculation without refinement. Multiscan empirical absorption was corrected using CrysAlisPro program (CrysAlisPro 1.171.38.41r, Rigaku Oxford Diffraction, 2015).

The structure refinement for [$\mathbf{Pd_2(L4Pyr)_2(OTf)_4}$] showed disordered electron density that could not be reliably modeled, therefore PLATON/SQUEEZE was used to remove the corresponding scattering contribution from the intensity data. This electron density can be attributed to solvent molecules (methyl *tert*-butyl ether) and anions missing atoms (CF_3SO_3 anions). The assumed solvent composition and missing anions atoms were used in the calculation of the empirical formula, formula weight, density, linear absorption coefficient, and F(000).

Crystallographic data for **L4Pyr**: $C_{42}H_{40}N_2S_4$, M = 701.00, orange needle, 0.272 × 0.099 × 0.054 mm^3, orthorhombic, space group $P2_12_12_1$, *a* = 4.9286(1) Å, *b* = 24.5232(3) Å, *c* = 30.1230(4) Å, V = 3640.8(1) Å^3, Z = 4, ρ_{calc} = 1.279 g/cm^3, μ = 2.640 mm^{-1}, *F*(000) = 1480, θ_{min} = 2.323°, θ_{max} = 76.681°, 14570 reflections collected, 7383 unique (R_{int} = 0.0223), parameters/restraints = 435/0, *R*1 = 0.0253 and w*R*2 = 0.0652 using

6964 reflections with $I > 2\sigma(I)$, $R1 = 0.0292$ and w$R2 = 0.0679$ using all data, GOF = 1.052, absolute structure parameter = −0.006(5), $-0.212 < \Delta\rho < 0.238$ e Å^{-3}. CCDC 1834510.

Crystallographic data for [**Pd$_2$(L4Pyr)$_2$(OTf)$_4$**]: $C_{352}H_{368}F_{24}Fe_4N_8O_{32}P_8Pd_4S_{24}$, M = 7344.72, red prism, 0.226 × 0.139 × 0.076 mm^3, triclinic, space group $P-1$, a = 20.4323(8) Å, b = 27.8575(11) Å, c = 32.2485(11) Å, α = 74.192(3)°, β = 88.216(3)°, γ = 87.829(3)°, V = 17644.6(12) Å^3, Z = 2, ρ_{calc} = 1.382 g/cm^3, μ = 5.192 mm^{-1}, $F(000)$ = 7600, θ_{min} = 2.454°, θ_{max} = 72.990°, 123021 reflections collected, 66698 unique (R_{int} = 0.1446), parameters/restraints = 3061/97, $R1 = 0.1257$ and w$R2 = 0.3112$ using 22013 reflections with $I > 2\sigma(I)$, $R1 = 0.2092$ and w$R2 = 0.3734$ using all data, GOF = 0.914, $-1.988 < \Delta\rho < 2.867$ e Å^{-3}. CCDC 1834511.

4. Conclusions

The synthesis and characterization of a M_2L_2 self-assembled metalla-macrocycle [**Pd$_2$(L4Pyr)$_2$(OTf)$_4$**] constructed from an electron-rich ligand **L4Pyr** and a square planar *cis*-blocked Pd(II) salt was demonstrated. This work illustrates once again the versatility and efficiency of the coordination-driven self-assembly strategy, when specific macrocyclic targets are focused. In contrast to M_2L_4 structure featuring the redox-active 9-(1,3-dithiol-2-ylidene)fluorene framework that was previously obtained from a pyridine-3-yl functionalized ligand [29], the present work depicts the construction of a totally different discrete M_2L_2 structure from a pyridine-3-yl functionalized ligand. The resulting [**Pd$_2$(L4Pyr)$_2$(OTf)$_4$**] complex features four electro-active units in total, i.e., two 9-(1,3-dithiol-2-ylidene)fluorene units which are independently and reversibly oxidized to the corresponding cation-radical (0.59 V vs. Fc/Fc^+), and two ferrocene moieties (0.83 V vs. Fc/Fc^+). The total charge of the metalla-ring can be therefore reversibly tuned between +4 and +8. Exploration of this capability to tune electrostatic interactions along host-guest processes is underway.

Supplementary Materials: The following are available online at http://www.mdpi.com/2304-6740/6/2/44/s1, NMR and ESI-FTICR mass spectra (Figures S1–S8), cif files and check cif files of **L4Pyr** and [**Pd$_2$(L4Pyr)$_2$(OTf)$_4$**].

Author Contributions: Sébastien Goeb and Marc Sallé conceived, designed the experiments, analyzed the data and wrote the paper; Serhii Krykun performed the experiments; Zoia Voitenko advises; Magali Allain performed X-ray analyses; Vincent Carré and Frédéric Aubriet performed ESI-FTICR analyses.

Acknowledgments: This work has been supported partially by the ANR JCJC program (ANR-14-CE08-0001 BOMBER). The authors gratefully acknowledge the MENRT for a PhD grant (VC) and the French Embassy in Kiev (Ukr) for a PhD grant (SK). They also acknowledge the ASTRAL platform (SFR MATRIX, Univ. Angers) for their assistance in spectroscopic analyses.

Conflicts of Interest: The authors declare no conflict of interest.

References

1. Fujita, M.; Yazaki, J.; Ogura, K. Preparation of a macrocyclic polynuclear complex, [(en)Pd(4,4′-bpy)]$_4$(NO$_3$)$_8$ (en = ethylenediamine, bpy = bipyridine), which recognizes an organic molecule in aqueous media. *J. Am. Chem. Soc.* **1990**, *112*, 5645–5647. [CrossRef]
2. Cook, T.R.; Stang, P.J. Recent developments in the preparation and chemistry of metallacycles and metallacages via coordination. *Chem. Rev.* **2015**, *115*, 7001–7045. [CrossRef] [PubMed]
3. Mishra, A.; Kang, S.C.; Chi, K.-W. Coordination-Driven Self-Assembly of Arene–Ruthenium Compounds. *Eur. J. Inorg. Chem.* **2013**, 5222–5232. [CrossRef]
4. Smulders, M.M.J.; Riddell, I.A.; Browne, C.; Nitschke, J.R. Building on architectural principles for three-dimensional metallosupramolecular construction. *Chem. Soc. Rev.* **2013**, *42*, 1728–1754. [CrossRef] [PubMed]
5. Young, N.J.; Hay, B.P. Structural design principles for self-assembled coordination polygons and polyhedra. *Chem. Commun.* **2013**, *49*, 1354–1379. [CrossRef] [PubMed]
6. Cook, T.R.; Zheng, Y.-R.; Stang, P.J. Metal–organic frameworks and self-assembled supramolecular coordination complexes: Comparing and contrasting the design, synthesis, and functionality of metal–organic materials. *Chem. Rev.* **2012**, *113*, 734–777. [CrossRef] [PubMed]
7. Chakrabarty, R.; Mukherjee, P.S.; Stang, P.J. Supramolecular coordination: Self-assembly of finite two-and three-dimensional ensembles. *Chem. Rev.* **2011**, *111*, 6810–6918. [CrossRef] [PubMed]

8. Zarra, S.; Wood, D.M.; Roberts, D.A.; Nitschke, J.R. Molecular containers in complex chemical systems. *Chem. Soc. Rev.* **2015**, *44*, 419–432. [CrossRef] [PubMed]
9. Amouri, H.; Desmarets, C.; Moussa, J. Confined nanospaces in metallocages: guest molecules, weakly encapsulated anions, and catalyst sequestration. *Chem. Rev.* **2012**, *112*, 2015–2041. [CrossRef] [PubMed]
10. Casini, A.; Woods, B.; Wenzel, M. The Promise of Self-Assembled 3D Supramolecular Coordination Complexes for Biomedical Applications. *Inorg. Chem.* **2017**, *56*, 14715–14729. [CrossRef] [PubMed]
11. Ahmad, N.; Younus, H.A.; Chughtai, A.H.; Verpoort, F. Metal–organic molecular cages: Applications of biochemical implications. *Chem. Soc. Rev.* **2015**, *44*, 9–25. [CrossRef] [PubMed]
12. Cook, T.R.; Vajpayee, V.; Lee, M.H.; Stang, P.J.; Chi, K.-W. Biomedical and biochemical applications of self-assembled metallacycles and metallacages. *Acc. Chem. Res.* **2013**, *46*, 2464–2474. [CrossRef] [PubMed]
13. Diaz-Moscoso, A.; Ballester, P. Light-responsive molecular containers. *Chem. Commun.* **2017**, *53*, 4635–4652. [CrossRef] [PubMed]
14. Wang, W.; Wang, Y.-X.; Yang, H.-B. Supramolecular transformations within discrete coordination-driven supramolecular architectures. *Chem. Soc. Rev.* **2016**, *45*, 2656–2693. [CrossRef] [PubMed]
15. McConnell, A.J.; Wood, C.S.; Neelakandan, P.P.; Nitschke, J.R. Stimuli-responsive metal–ligand assemblies. *Chem. Rev.* **2015**, *115*, 7729–7793. [CrossRef] [PubMed]
16. Qu, D.-H.; Wang, Q.-C.; Zhang, Q.-W.; Ma, X.; Tian, H. Photoresponsive host–guest functional systems. *Chem. Rev.* **2015**, *115*, 7543–7588. [CrossRef] [PubMed]
17. Croué, V.; Goeb, S.; Sallé, M. Metal-driven self-assembly: The case of redox-active discrete architectures. *Chem. Commun.* **2015**, *51*, 7275–7289. [CrossRef] [PubMed]
18. Xu, L.; Wang, Y.-X.; Chen, L.-J.; Yang, H.-B. Construction of multiferrocenyl metallacycles and metallacages via coordination-driven self-assembly: From structure to functions. *Chem. Soc. Rev.* **2015**, *44*, 2148–2167. [CrossRef] [PubMed]
19. Szalóki, G.; Croué, V.; Carré, V.; Aubriet, F.; Aleveque, O.; Levillain, E.; Allain, M.; Arago, J.; Orti, E.; Goeb, S.; et al. Controlling the Host–Guest Interaction Mode through a Redox Stimulus. *Angew. Chem. Int. Ed.* **2017**, *56*, 16272–16276. [CrossRef] [PubMed]
20. Croué, V.; Goeb, S.; Szalóki, G.; Allain, M.; Sallé, M. Reversible Guest Uptake/Release by Redox-Controlled Assembly/Disassembly of a Coordination Cage. *Angew. Chem. Int. Ed.* **2016**, *55*, 1746–1750. [CrossRef] [PubMed]
21. Szalóki, G.; Croué, V.; Allain, M.; Goeb, S.; Sallé, M. Neutral versus polycationic coordination cages: A comparison regarding neutral guest inclusion. *Chem. Commun.* **2016**, *52*, 10012–10015. [CrossRef] [PubMed]
22. Bivaud, S.; Goeb, S.; Croué, V.; Allain, M.; Pop, F.; Sallé, M. Tuning the size of a redox-active tetrathiafulvalene-based self-assembled ring. *Beilstein J. Org. Chem.* **2015**, *11*, 966–971. [CrossRef] [PubMed]
23. Vajpayee, V.; Bivaud, S.; Goeb, S.; Croué, V.; Allain, M.; Popp, B.V.; Garci, A.; Therrien, B.; Sallé, M. Electron-Rich Arene–Ruthenium Metalla-architectures Incorporating Tetrapyridyl–Tetrathiafulvene Donor Moieties. *Organometallics* **2014**, *33*, 1651–1658. [CrossRef]
24. Bivaud, S.; Goeb, S.; Croué, V.; Dron, P.I.; Allain, M.; Sallé, M. Self-assembled containers based on extended tetrathiafulvalene. *J. Am. Chem. Soc.* **2013**, *135*, 10018–10021. [CrossRef] [PubMed]
25. Bivaud, S.; Balandier, J.Y.; Chas, M.; Allain, M.; Goeb, S.; Sallé, M. A metal-directed self-assembled electroactive cage with bis(pyrrolo) tetrathiafulvalene (BPTTF) side walls. *J. Am. Chem. Soc.* **2012**, *134*, 11968–11970. [CrossRef] [PubMed]
26. Goeb, S.; Bivaud, S.; Dron, P.I.; Balandier, J.-Y.; Chas, M.; Sallé, M. A BPTTF-based self-assembled electron-donating triangle capable of C_{60} binding. *Chem. Commun.* **2012**, *48*, 3106–3108. [CrossRef] [PubMed]
27. Perepichka, D.F.; Perepichka, I.F.; Ivasenko, O.; Moore, A.J.; Bryce, M.R.; Kuz'mina, L.G.; Batsanov, A.S.; Sokolov, N.I. Combining High Electron Affinity and Intramolecular Charge Transfer in 1,3-Dithiole–Nitrofluorene Push–Pull Diads. *Chem. Eur. J.* **2008**, *14*, 2757–2770. [CrossRef] [PubMed]
28. Amriou, S.; Wang, C.; Batsanov, A.S.; Bryce, M.R.; Perepichka, D.F.; Ortí, E.; Viruela, R.; Vidal-Gancedo, J.; Rovira, C. The Interplay of Inverted Redox Potentials and Aromaticity in the Oxidized States of New π-Electron Donors: 9-(1,3-Dithiol-2-ylidene) fluorene and 9-(1,3-Dithiol-2-ylidene) thioxanthene Derivatives. *Chem. Eur. J.* **2006**, *12*, 3389–3400. [CrossRef] [PubMed]
29. Croué, V.; Krykun, S.; Allain, M.; Morille, Y.; Aubriet, F.; Carré, V.; Voitenko, Z.; Goeb, S.; Sallé, M. A self-assembled M_2L_4 cage incorporating electron-rich 9-(1,3-dithiol-2-ylidene) fluorene units. *New J. Chem.* **2017**, *41*, 3238–3241. [CrossRef]

30. Cohen, Y.; Avram, L.; Frish, L. Diffusion NMR spectroscopy in supramolecular and combinatorial chemistry: An old parameter—New insights. *Angew. Chem. Int. Ed.* **2005**, *44*, 520–554. [CrossRef] [PubMed]
31. Shanmugaraju, S.; Vajpayee, V.; Lee, S.; Chi, K.-W.; Stang, P.J.; Mukherjee, P.S. Coordination-driven self-assembly of 2d-metallamacrocycles using a new carbazole-based dipyridyl donor: Synthesis, characterization, and C_{60} binding study. *Inorg. Chem.* **2012**, *51*, 4817–4823. [CrossRef] [PubMed]
32. Mishra, A.; Ravikumar, S.; Hong, S.H.; Kim, H.; Vajpayee, V.; Lee, H.; Ahn, B.; Wang, M.; Stang, P.J.; Chi, K.-W. DNA binding and unwinding by self-assembled supramolecular heterobimetallacycles. *Organometallics* **2011**, *30*, 6343–6346. [CrossRef] [PubMed]
33. Ferrer, M.; Gutiérrez, A.; Rodríguez, L.; Rossell, O.; Ruiz, E.; Engeser, M.; Lorenz, Y.; Schilling, R.; Gómez-Sal, P.; Martín, A. Self-assembly of heterometallic metallomacrocycles via ditopic fluoroaryl gold (I) organometallic metalloligands. *Organometallics* **2012**, *31*, 1533–1545. [CrossRef]
34. Niu, Z.; Li, D.; Liu, D.; Xia, D.; Zou, Y.; Sun, W.; Li, G. Syntheses, electrochemical behaviors, spectral properties and DFT calculations of two 1,3-dithiole derivatives. *Chem. Res. Chin. Univ.* **2014**, *30*, 425–430. [CrossRef]
35. Zhao, Y.-P.; Wu, L.-Z.; Si, G.; Liu, Y.; Xue, H.; Zhang, L.-P.; Tung, C.-H. Synthesis, spectroscopic, electrochemical and Pb^{2+}-binding studies of tetrathiafulvalene acetylene derivatives. *J. Org. Chem.* **2007**, *72*, 3632–3639. [CrossRef] [PubMed]
36. Estrada, L.A.; Neckers, D.C. Synthesis and photophysics of ambipolar fluoren-9-ylidene malononitrile derivatives. *J. Org. Chem.* **2009**, *74*, 8484–8487. [CrossRef] [PubMed]
37. Broman, S.L.; Andersen, C.L.; Jousselin-Oba, T.; Manso, M.; Hammerich, O.; Frigoli, M.; Nielsen, M.B. Tetraceno [2,1,12,11-opqra] tetracene-extended tetrathiafulvalene–redox-controlled generation of a large PAH core. *Org. Biomol. Chem.* **2017**, *15*, 807–811. [CrossRef] [PubMed]